Novel phases in ammonia-water mixtures under pressure

Novel phases in ammonia-water mixtures under pressure

Victor Naden Robinson,[1] Miriam Marqués,[1] Yanchao Wang,[2,3] Yanming Ma,[2,3,4] and Andreas Hermann[1,*]

[1] *Centre for Science at Extreme Conditions and SUPA, School of Physics and Astronomy, The University of Edinburgh, Edinburgh EH9 3FD, United Kingdom*

[2] *State Key Laboratory for Superhard Materials, Jilin University, Changchun 130012, China*

[3] *Innovation Center for Computational Physics Methods and Software, College of Physics, Jilin University, Changchun 130012, China*

[4] *International Center for Future Science, Jilin University, Changchun 130012, China*

(Dated: November 26, 2018)

Abstract

While ammonia and water readily form hydrogen-bonded molecular mixtures at ambient conditions, their miscibility under pressure is not well understood, yet crucial e.g. to model the interior of icy planets. We report here on the behaviour of ammonia-water mixtures under extreme pressure conditions, based on first-principles calculations of 15 stoichiometries in the pressure range of 1 atm to 10 Mbar. We show that compression facilitates proton transfer from water to ammonia in all relevant mixtures. This favors ammonia-rich hydrates above 1 Mbar, stabilized by complete de-protonation of water and the formation of the unusual structural motifs $O^{2-}\cdot(NH_4^+)_2$ and $O^{2-}\cdot(N_2H_7^+)_2$. The hydronitrogen cations persist to the highest pressures studied. We predict a new ammonia-rich 4:1-hydrate at intermediate pressures and find that by 5.5 Mbar, close to the core-mantle boundary of Neptune, all cold ammonia-water mixtures are unstable against decomposition into their constituents.

* a.hermann@ed.ac.uk

I. INTRODUCTION

Mixtures of molecular ices of water, ammonia and methane (together with impurities and volatiles such as hydrogen or helium) make up a large proportion of the mantle regions of the "ice giants" Uranus and Neptune as well as large icy moons in our solar system, and are presumed to feature prominently in the large number of Neptune-like exoplanets discovered by recent and ongoing astronomical observation campaigns.[1–5] It is not clear how molecular ices organize themselves inside these planetary bodies – whether they form segregated layers with distinct chemical and density profiles, or homogeneous mixtures corresponding roughly to the global composition ratio throughout. High pressure conditions (which reach hundreds of GPa, or several Mbar, inside ice giants) can in general favor unexpected chemical motifs, and thus stabilize unusual compounds and stoichiometries, as found among prototypical mineral compounds[6–10] as well as individual ices.[11–16]

The molecular ices exhibit very different chemical responses to pressure: water ice forms a sequence of atomic networks above 65 GPa, where water molecules readily give up their protons to sit at the mid-points of nearest-neighbor O–O separations,[13, 14, 17, 18] while ammonia holds onto its protons much better, and instead self-ionizes above 120 GPa into ammonium amide over a large pressure range before (in calculations) returning to packings of neutral molecules.[15, 16, 19] The *mixtures* of the molecular ices can feature surprising pathways to stability under compression; for instance, methane's solubility in water increases to about 40% at pressures as low as a few GPa,[20] which is largely unexplained. Mixtures of ammonia and water are of particular interest, as they can form hydrogen-bonded networks. First-principles calculations have so far proven very useful in establishing or confirming the phase diagrams and properties of the individual ices and of a select few hydrate phases. Here, we present a computational study of the entire binary ammonia-water phase diagram that considers *all* mutual formation and decomposition reactions at various pressures and temperatures, and also establishes which *new* hydrate stoichiometries should be stabilized under particular conditions.

II. COMPUTATIONAL METHODOLOGY

Solid crystalline structures were searched for using the particle swarm optimization algorithm as implemented in CALYPSO (crystal structure analysis by particle swarm optimization).[21, 22] Structure predictions were performed with up to 16 formula units of $(H_2O)_X(NH_3)_Y$, where X and Y are integers, and at 5, 10, 20, 30, 50, 80, and 100 – 1000 GPa in increments of 100 GPa. These searches were performed for the three canonical ammonia-water mixing ratios. At 50, 100, and 300 GPa binary searches were performed to look for other stable mixing ratios. If a new mixing ratio was found to be stable, further searches were performed for this stoichiometry at relevant pressures. Structure predictions at pressures over 1 TPa and up to 5 TPa failed to find any structures stable against decomposition into NH_3 and H_2O. The predicted decomposition of NH_3 above 460 GPa was taken into account throughout.[23]

Electronic structure calculations, geometry optimizations, and phonon calculations were performed with the CASTEP code [24]. Exchange-correlation effects were described within the generalized gradient approximation (GGA) using the Perdew-Burke-Ernzerhof (PBE) functional [25] unless otherwise stated, and ultrasoft pseudopotentials. Final structure relaxations were done with "hard" pseudopotentials with cutoff radii no greater than 1.2 Å for oxygen and nitrogen, and 0.6 Å for hydrogen. Plane wave cutoffs of $E_c = 1000$ eV and k-point spacings of $20/\text{Å}^{-1}$ were found to give sufficiently converged energies and forces.

Phase stabilities at finite temperature were determined by calculating free energies from lattice vibrations within the harmonic approximation. Phonon calculations were also used to produce phonon dispersions, and zone-centered phonon frequencies to predict Infrared and Raman spectroscopic signals. Bader and electron localization function (ELF) analyses used real-space scalar fields obtained with the VASP code in conjunction with 'hard' projector-augmented wave frozen core data sets,[26, 27] which were analysed with the Critic2 code (see the Supplemental Material, SM, for details).[28] Molecular calculations for water-ammonia dimers and trimers used the Gaussian09 software package and aug-cc-pVTZ basis sets.[29, 30]

III. RESULTS

Three stoichiometric ammonia hydrates exist in nature and have been explored around ambient and low-pressure conditions: ammonia monohydrate (AMH, NH_3:H_2O=1:1), ammonia dihydrate (ADH, 1:2) and ammonia hemiydrate (AHH, 2:1).[31, 32] For comparison, the ammonia:water solar abundance ratio is 1:7.[33] The three hydrates' phase diagrams show appreciable complexity: at various $P-T$ conditions, five solid AMH and ADH phases, as well as three solid AHH phases have been identified in experiment, even though some of their structures have not been resolved. Those we know are hydrogen-bonded molecular crystals. There is some interplay between the three mixtures: both ADH and AMH decompose into AHH and ice-VII, around 3 GPa and at 280 K and 250 K, respectively, while ADH also decomposes into AMH and ice-VII around 0.55 GPa and 190 K.[34–36] Around 5–20 GPa and room temperature, *all* ammonia hydrates are found to form disordered molecular alloy (DMA) phases, with substitutional disorder of ammonia and water on a body-centered cubic (bcc) lattice and possibly partial ionization into OH^-/NH_4^+.[34, 37–40] Moreover, first-principles calculations predict the appearance of ionic phases, where proton transfer leads to the formation of hydroxyl and ammonium groups, in *all* hydrates at elevated pressures.[41–44] The highest pressure any hydrate has been studied in experiment is 41 GPa.[45] Here, we begin by discussing individually the calculated high-pressure and -temperature phase evolution of the three known ammonia hydrates.

Ammonia monohydrate, AMH. Two low-pressure, low-temperature phases of AMH, AMH-I and AMH-II, have been fully resolved.[31, 46, 47] A computational prediction by Griffiths *et al.* suggests that a tetragonal ionic ammonium hydroxide phase, $(OH^-)(NH_4^+)$, becomes more stable than AMH-II above 2.8 GPa.[43] Only an incomplete transformation into this phase has been observed experimentally, which is possibly frustrated due to the substitutional disorder in the DMA phase.[40] The high-pressure phase evolution of AMH has recently been studied computationally by Bethkenhagen *et al.*, who used crystal structure prediction to identify relevant solid phases, which were then used as initial configurations for molecular dynamics (MD) simulations.[48] The ground state high-pressure phases found in this way proved important to obtain accurate equations-of-state data at high temperatures.[48]

In the left panel of Figure 1 we show the enthalpies of formation of the known AMH

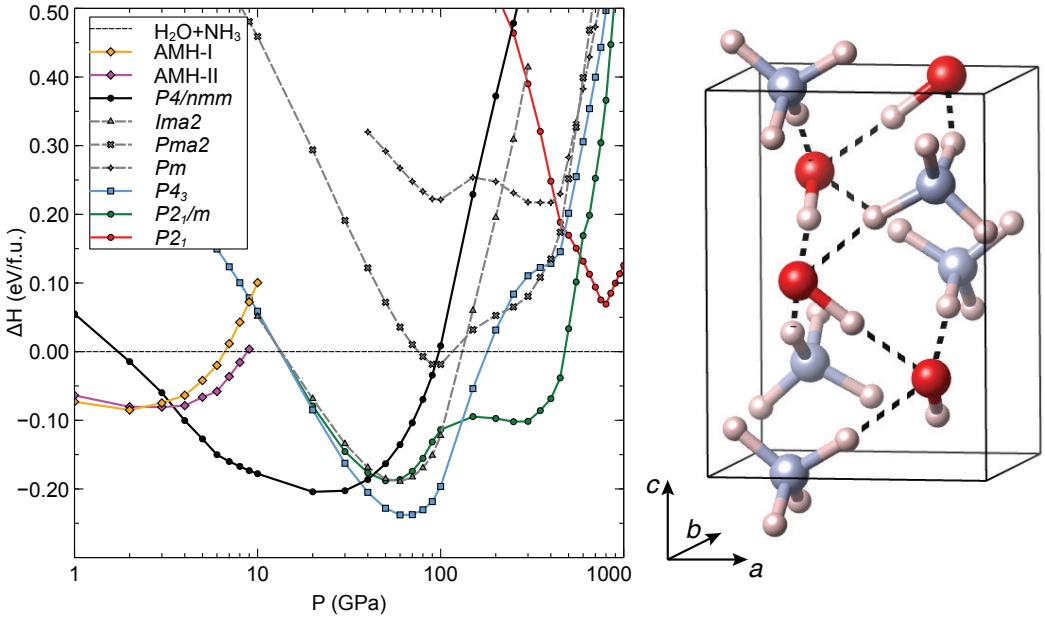

FIG. 1. Left: relative ground state enthalpies of AMH per formula unit, relative to decomposition into NH_3 and H_2O. Black circles show the $P4/nmm$ phase reported by Griffiths *et al.*,[43] and gray symbols are phases reported by Bethkenhagen *et al.*[48] Right: AMH-$P4_3$ at 50 GPa. Red (blue, pink) spheres denote O (N, H) atoms, and covalent bonds are indicated. Hydrogen bonds are shown by bashed black lines.

phases, the structures proposed by Griffiths *et al.* and (in gray symbols) by Bethkenhagen *et al.*, and from our own structure searches, all drawn relative to decomposition into pure water and ammonia ice. We confirm the literature findings regarding phase succession and transition pressures. All predicted high-pressure phases are ionic, of the form $(OH^-)(NH_4^+)$, and represent different arrangements of the ammonium and hydroxyl groups. However, note from Figure 1 that these previously reported phases become unstable towards decomposition into pure water and ammonia above 120 GPa. This would make AMH, its appealing simple stoichiometry notwithstanding, much less important inside icy planets' mantles than hitherto thought. Our own structure searches uncovered a sequence of high-pressure phases that are, above 35 GPa, more stable than those proposed in the literature. Most importantly, these structures shift the decomposition of AMH into the pure ices to almost 500 GPa in the ground state.

We find two new phases that are relevant over this large pressure range: a tetragonal $P4_3$ structure from 35 to 140 GPa, and a monoclinic $P2_1/m$ phase between 140 and 470 GPa.

The $P4_3$ phase, like the $P4/nmm$ phases it supersedes, is an ionic structure that comprises OH^- and NH_4^+ groups. The hydroxyl groups in the $P4_3$ phase form chiral hydrogen-bonded spirals (see Figure 1); in comparison to the $P4/nmm$ structure, with linear O-H$\cdots$O-H chains, and the $Ima2$ structure, with planar zig-zag O-H$\cdots$O-H chains, this leads to a more compact overall arrangement. The molecular units of $P4_3$ are arranged overall in what can be interpreted as a quasi-bcc layout. The $P4_3$ structure therefore seems to be an ordered (and ionic) variant of the DMA phase observed experimentally at high temperatures. A proper model of the DMA phase would require the analysis of all possible microscopic configurations in adequate supercells of the DMA's body-centered cubic heavy atom lattice, and their occupancy at given temperatures to compare free energies. A recent combined experimental and computational study of AMH-DMA reported diffractive and spectroscopic properties of low-energy candidates for this phase from (4,4,4) supercell calculations.[40]

At 140 GPa a monoclinic ionic $P2_1/m$ structure (8 f.u./cell) becomes more stable than $P4_3$ and remains the most stable AMH phase over a large pressure range, up to 470 GPa. In this phase, protons of hydroxyl groups are positioned close to the mid-points along O–H–O bonds, and those form one-dimensional chains along the a axis, see the SM. These O-H chains are themselves arranged in a matrix of NH_4^+ cations, a structural motif for instance seen in the high-pressure phases of the alkali hydroxides (Rb,Cs)OH.[49, 50] In half of the O-H chains the O–H–O connections are symmetric and linear, while in the other half they are asymmetric and bent, and form hydrogen-bonded (H_2O)–O. With increased pressure, the $P2_1/m$ phase continuously adopts a higher symmetry $P2_12_12_1$ phase with a half-sized unit cell, and where all O–H–O bonds are symmetric and buckled. Above 470 GPa, the $P2_1/m$ phase is no longer stable with respect to decomposition into the molecular ices, and we find no other stable AMH phases in our searches. In the SM we show the P-T phase diagram of AMH, constructed from free energies that include vibrational entropies at the harmonic level.

AMH thus has a richer phase diagram than previously assumed. A set of newly predicted phases extends its stability against decomposition into the ices from 120 GPa to 470 GPa. These new phases are a sequence of ionic structures $(OH^-)\cdot(NH_4^+)$ with ever more compact arrangements and eventual formation of one-dimensional symmetric –[–O–H–]– chains in an ammonium matrix.

Ammonia dihydrate, ADH. ADH, of the ammonia hydrates known at ambient condi-

tions, is the most water-rich and closest to the solar abundance ratio of water and ammonia, and could therefore be of significance at extreme conditions. Three of its solid phases, including the DMA phase, have been solved,[31, 38, 46, 51] with ADH-IV still to be clarified, although its unit cell dimensions have been reported.[35] A recent DFT study suggested the formation of an ionic phase, $(NH_4^+)(OH^-)(H_2O)$, at 12 GPa, which was reported to be stable up to at least 45 GPa.[44] However, we find the ADH phase diagram to be somewhat richer, see Figure 2.

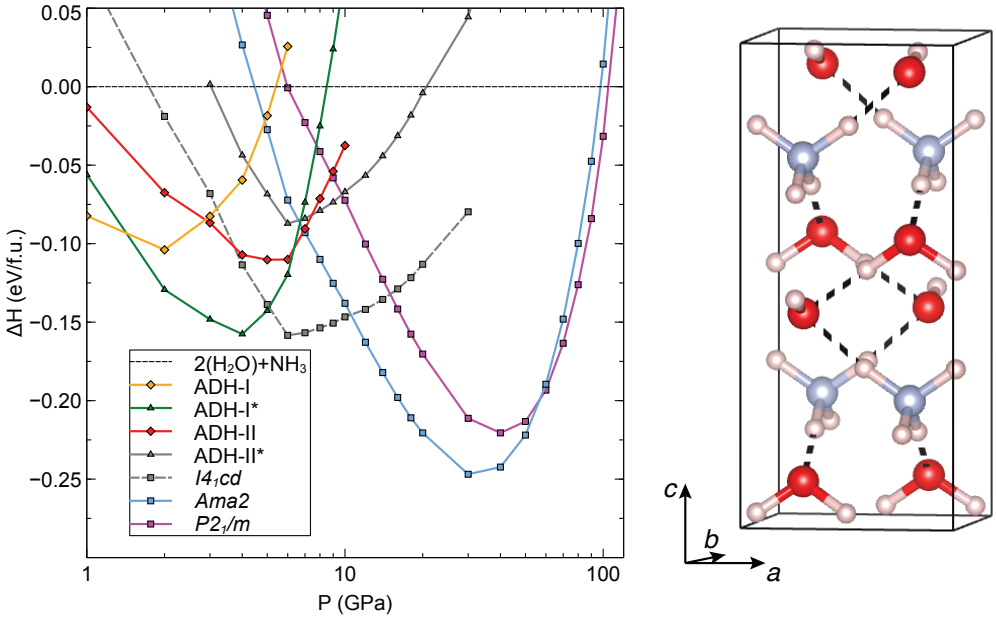

FIG. 2. Left: relative ground state enthalpies of ADH per formula unit, relative to decomposition into NH_3 and H_2O. Right: ADH-*Ama*2 at 20 GPa.

At low pressures, we find ADH-I to be most stable; it would be superseded by ADH-II at ∼3 GPa if not for the emergence of an ionic variant of ADH-I. This phase, which we call ADH-I* here, emerges through a proton transfer along a particular hydrogen bond, HO-H···NH_3 → HO···H-NH_3, equivalent to that seen in early calculations on compressed AMH and AHH.[41, 42] The molecular ADH-II phase has a similar transition to an ionic variant ADH-II* above 7 GPa; see the SM for both structures. The ADH-I* phase is stable from 1.5 to 5 GPa in our calculations and completely displaces the known ADH-II phase from stability. Above 5 GPa the recently suggested $I4_1cd$ phase becomes more stable. In our calculations, however, that phase remains only stable up to 10 GPa, where we find a new orthorhombic *Ama*2 phase to become more stable; and finally a monoclinic $P2_1/m$ phase

stable above 60 GPa. The $Ama2$ (see Figure 2) and $P2_1/m$ phases (see the SM) extend the stability region of ADH towards decomposition into the ices to over 100 GPa. However, neither the tetragonal $I4_1cd$ phase (with $Z = 16$ molecules per cell) nor the base-centered orthorhombic $Ama2$ phase (with $Z = 4$) match the suggestion for ADH-IV based on neutron diffraction data (primitive orthorhombic lattice with $Z = 8$).[35]

As in AMH, ionization of water molecules becomes preferable in ADH under pressure, and the ADH-I*, $I4_1cd$, $Ama2$, and $P2_1/m$ phases all can be seen as $(OH^-)(NH_4^+)(H_2O)$. The latter three all arrange in layered structures, as can be seen in Figure 2: along the c^* axis they feature alternate layers of NH_4^+, OH^-, and H_2O. Overall, this optimizes electrostatic interactions, as the ionic components NH_4^+ and OH^- are adjacent, while the water dipole moments are aligned along the local electric field established by adjacent ammonium and hydroxyl layers. In addition, all structures are fully hydrogen bonded: all NH_4^+ groups donate four hydrogen bonds; all water molecules donate and accept two bonds, respectively; and all OH^- groups donate one hydrogen bond and accept four. Eventually, however, and at much lower pressures than in AMH (and AHH, see next subsection), ADH becomes unstable towards decomposition into the ices.

Ammonia hemihydrate, AHH. The AHH mixture, with twice as high ammonia content as AMH, is farthest removed from the solar abundance ratio of water and ammonia, and thus seems much less relevant for interiors of planets. However, AHH forms as part of decompositions of both AMH and ADH, hinting at its relative stability.[34, 36] While its three known solid phases have been solved using neutron diffraction,[31, 36, 39, 46] their respective regions of stability are less well established than for the other hydrates, and there are indications for high-pressure phase transitions beyond 30–40 GPa that have yet to be identified.[45]

We have recently shown that the 2:1 stoichiometry of AHH allows for the formation of completely ionic ammonium oxide structures, $O^{2-}(NH_4^+)_2$.[52] At low pressures, we reproduce the stability of AHH-I followed by AHH-II (see Figure 3). We then find several enthalpically similar phases in the pressure region of 35–65 GPa, with the common features of quasi-bcc arrangement of the molecular units and half-ionization, i.e., all these phases are $(OH^-)(NH_4^+)(NH_3)$. Above 65 GPa, however, a different motif emerges, where all stable phases have completely deprotonated water, and form fully ionic ammonium oxide structures. A sequence of structures of composition $O^{2-}(NH_4^+)_2$ is stable in the ground state up

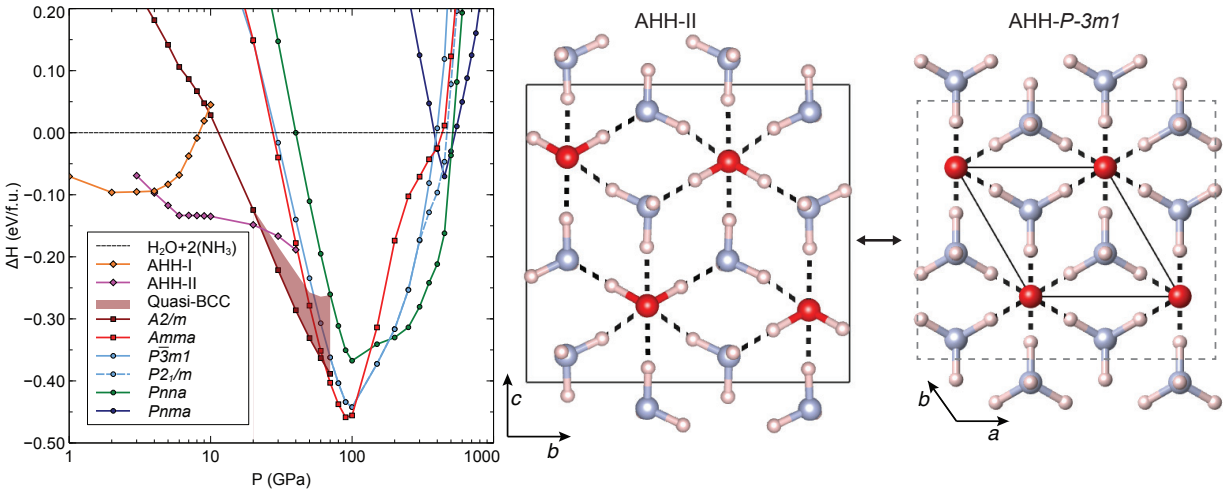

FIG. 3. Left: relative ground state enthalpies of AHH per formula unit, relative to decomposition into NH_3 and H_2O. Right: AHH-II at 10 GPa and $P\bar{3}m1$ at 150 GPa. Solid black lines indicate their primitive unit cells; the grey dashed line in AHH-$P\bar{3}m1$ points out its relation to the unit cell of the AHH-II phase (see text).

to 550 GPa. In fact, in calculations compressed AHH-II spontaneously ionizes to form the $P\bar{3}m1$ phase as shown in Figure 3.

If we include ZPE and vibrational entropy effects for all phases to obtain free energies (see the SM), we find that the onset of stability for the ionic phases is reduced to 40 GPa at room temperature; that the simple $P\bar{3}m1$ phase (isostructural to the ionic CdI_2 structure) has a much extended stability range; and that eventual decomposition is predicted at somewhat lower pressures, around 450–550 GPa.

New ammonia-rich hydrate under pressure. So far, we have discussed the hydrates individually, and only stated their stability against decomposition into the constituent ices. However, other reactions can and must be considered – some are already known from experimental studies: both molecular AMH and ADH decompose into AHH-II and excess ice-VII/VIII. All possible reactions can be summarized very succinctly in a convex hull diagram. There, we plot the relative enthalpy of formation for an arbitrary hydrate AXH, which shall be $(H_2O)_{1-x}(NH_3)_x$, against its relative ammonia content x:

$$\Delta H_f(x) = H_f(\mathrm{AXH}) - (1-x)H_f(\mathrm{H_2O}) - xH_f(\mathrm{NH_3}) \tag{1}$$

The compounds whose enthalpies form the *convex hull* of $\Delta H_f(x)$ are stable against decomposition into any other binary mixture of ammonia and water, at the given external pressure

conditions. While so far we only considered $x = 1/3$, $1/2$, and $2/3$, ammonia hydrates could in principle take up many other compositions. We therefore performed crystal structure searches across the entire binary H_2O–NH_3 phase diagram, at 50, 100, and 300 GPa. Those pressures were chosen to correspond to the emergence of (half-)ionic phases across all hydrates, the predicted destabilization of ADH, and the region of stability of fully ionic phases in AHH, respectively.

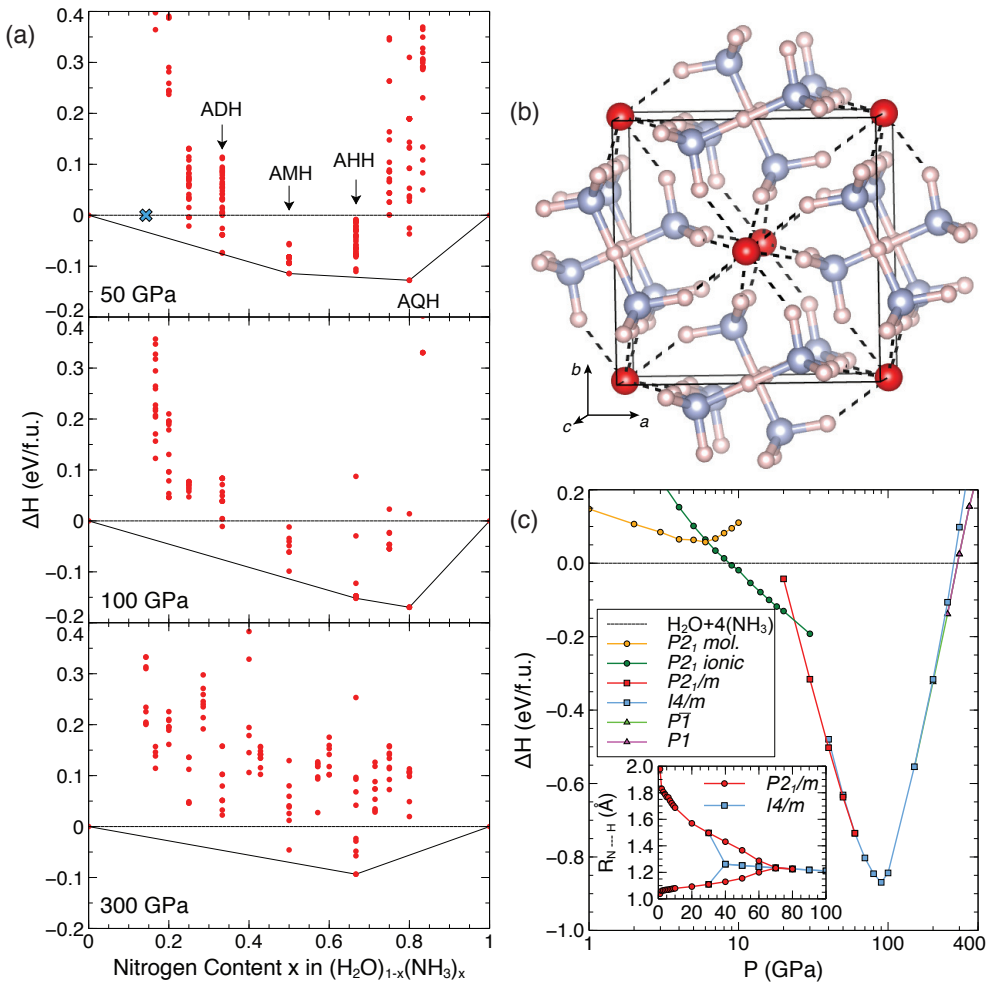

FIG. 4. (a) Relative formation enthalpies $\Delta H_f(x)$ for ammonia-water mixtures found in crystal structure searches at 50, 100, and 300 GPa, with up to 50 structures shown for each composition. The solar abundance ratio of ammonia to water is indicated by the blue cross. (b) The AQH-$I4/m$ structure at 100 GPa. (c) Ground state enthalpies per formula unit of AQH relative to the constituent ices; inset shows covalent and hydrogen-bonded N-H separations in $N_2H_7^+$.

In Figure 4(a) we show $\Delta H_f(x)$ for the best candidate structures that emerged from

the structure searches. The figure shows that a focus on individual hydrates and ices is insufficient. For instance, at 100 GPa all three known hydrates have negative enthalpies of formation ($\Delta H_f < 0$), but only AHH ($x = 2/3$) is part of the convex hull. Taking the most relevant phases for each composition from these search results and optimizing them across the entire pressure range allows us to predict the formation and decomposition conditions for each individual compound, which will be discussed in detail in the next subsection.

A very intriguing feature of Figure 4 is the emergence of a new ammonia-rich hydrate with $x = 0.8$: the 4:1 ammonia quarterhydrate ("AQH") $(NH_3)_4(H_2O)$ was found at 50 and 100 GPa. A representative structure of this compound is shown in Figure 4(b).

AQH become more stable than the ices at 8.5 GPa in a partially ionic monoclinic $P2_1$ phase, see Figure 4(c). This phase contains NH_3, NH_4^+, and OH^- units. Above 25 GPa, we find another monoclinic phase, $P2_1/m$ that, like AHH phases in a similar pressure range, features fully deprotonated water molecules – effectively forming $O^{2-}(NH_4^+)_2(NH_3)_2$. The spherically symmetric O^{2-} anion acts as an efficient hydrogen-bond acceptor: in AQH-$P2_1/m$, each oxygen atom accepts 12 hydrogen bonds from NH_3/NH_4 units. The ammonium and ammonia molecules are themselves hydrogen-bonded as $H_3N\text{-}H^+\cdots NH_3$. These hydrogen bonds symmetrize just above 60 GPa, thus forming H_3N–H–NH_3 units with a proton at the mid-point between two NH_3 molecules. Now in a higher symmetry tetragonal $I4/m$ structure, these $N_2H_7^+$ cations are stacked above each other along the c axis, rotated by 90° to minimize steric repulsion and maximise hydrogen bonding to the oxygen anions, see Figure 4(b). Within the ab plane, the cations are in a herringbone arrangement for the same reason. The high hydrogen-bond coordinations of the oxygen atoms remain.

The $N_2H_7^+$ cation has not been seen before in any ammonia hydrates, but forms as part of the ammonia adduct of ammonium iodide, $NH_4I{\cdot}NH_3$.[53–55] There, the cation is in the symmetry-broken $H_3N\text{-}H^+\cdots NH_3$ state, and takes up a rotationally disordered position in a CsCl-like structure, together with the counterion I^-. In AQH, the structure deviates from a simple ionic structure to optimize packing of the non-spherical $N_2H_7^+$ cations under compression.

Above 200 GPa, we find that a sequence of symmetry-reductions (to $P\bar{1}$ and then $P1$) lower the enthalpy of AQH with respect to the $I4/m$ structure. At 300 GPa, decomposition into the ices becomes favourable again, see Figure 4(b). The P-T phase diagram from harmonic free energies is shown in the SM. The structural sequence is unaffected by entropic

effects, but decomposition into the ices is predicted to occur slightly earlier than in the ground state, around 240 GPa at low temperatures.

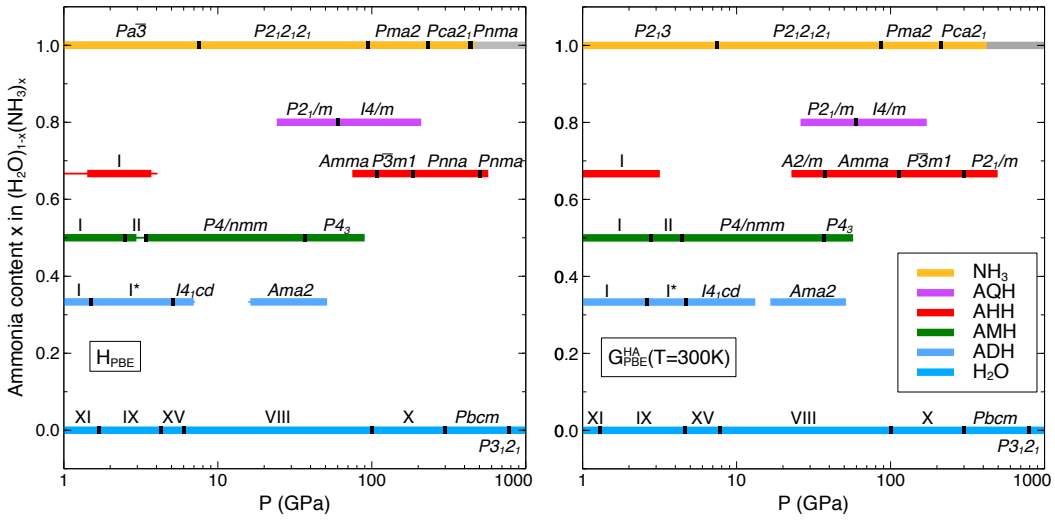

FIG. 5. Phase stability ranges for binary ammonia-water mixtures as function of pressure, for the ground state (left) and at $T = 300$ K (right). Stable compounds are labelled by commonly used numerals or space groups, black separators signify phase transitions. For pure ammonia, the gray region denotes decomposition into NH_4 and N_3H_7. Thin lines denote pressure regions where a phase is metastable (here defined as within 5 meV/molecule above the convex hull).

Full ammonia-water phase diagrams. From the convex hull diagrams we obtain stability ranges for all individual ammonia-water mixtures under pressure. Those stability ranges are displayed in Figure 5, both for the ground state and at room temperature. The latter include lattice vibrational entropic effects within the harmonic approximation, applied to all compounds. In both cases, coloured bars correspond to regions of stability of the various mixtures. Their end points (or intermediate gaps) signal that a specific mixture becomes unstable against one or more decomposition reactions, which we discuss below for every mixture involved.

In the ground state, we find AMH to be stable from $P = 1$ atm up to 85 GPa. The transition from AMH-I to AMH-II, in experiment seen around 0.5 GPa, happens in our calculations at 2.5 GPa. Above 85 GPa, AMH decomposes into the highly stable ionic AHH phases and ice. The upper limit of stability of AMH is thus much lower than if only the constituent ices were considered (470 GPa). Based on room temperature free energies, we

predict that AMH should decompose at even smaller pressures, around 60 GPa.

For the other hydrates, we find similar stability constraints due to non-trivial decomposition reactions. We find ADH to be initially unstable, but stable in the region $P = 0.5 \ldots 6.6$ GPa, and $P = 17.2 \ldots 48.5$ GPa. Due to the emergence of half-ionic ADH-I*, the experimentally known phase ADH-II does not appear in our calculated phase diagrams. In the intermediate pressure region, and also above its maximum point of stability, ADH is found unstable against decomposition into AMH and ice. This agrees with experiment, which finds a strongly temperature dependent decomposition of ADH-IV into AMH and ice at pressures 2.5-6.5 GPa.[56] However, experiments find the ADH-DMA phase (which we can not model here) at pressures above 6.5 GPa,[34, 38] which marks a re-entrant stability of ADH at high pressures. The newly found $Ama2$ phase represents such a re-entrant region of stability for ADH and is responsible in our calculations for an extension of ADH stability to almost 50 GPa.

AHH is found stable at $P = 1.5 \ldots 3.5$ GPa in the ground state and again from $P = 79 \ldots 540$ GPa, where decomposition into the ices eventually takes place. Here, the intermediate pressure instability is also due to the decomposition into AMH and ice. While AHH-I is correctly found stable, the high-pressure phase AHH-II does also not appear on the phase diagrams. In fact, we find both ADH and AHH unstable in certain regions of the phase diagram (at 6.6–17.2 GPa and 3.5–79 GPa) where neither has been found in experiment to decompose. While these discrepancies could in part be due to our calculations not including satisfactory structural models for some of the phases relevant in these pressure regions (such as ADH-IV and ADH-DMA) we also find that calculated regions of instability are considerably smaller when considering room temperature free energies (12.5–17 GPa and 3–24 GPa). This suggests that the ionic $P4/nmm$-AMH structure is energetically very stable in the ground state (leading to spurious metastability of both ADH and AHH), but not so dominant at elevated temperatures. Note that we have not considered anharmonic corrections to the phonon frequencies in this work. Proton transfers are responsible for several of the new ammonia hydrate phases, and the vibrational properties of the different chemical species thus created might have different anharmonic correction terms. The anharmonicity of the O–H and N–H stretch modes most notably could lead to different ZPE terms and free energies that affect the relative stability of the half- or fully ionic phases.[57, 58] That said, it is also possible that low-temperature compression experiments on ADH and AHH

might fail to overcome kinetic barriers towards decomposition into AMH and ice, just like compressed AMH itself might be unable to convert to the $P4/nmm$ phase.[40]

The new AQH is stable in the ground state from 25.5 . . . 198 GPa. At either end of this pressure range, a decomposition into AHH and excess ammonia is more stable. Like AHH, the AQH structures across their stability range benefit from strong ionic interactions and high coordination upon formation of the unusual $N_2H_7^+$ cation. Our results suggest that AQH can be synthesised in a high-pressure reaction of a 2:1 molar mixture of ammonia and AHH.

The discrepancies between our calculations and the experimental phase diagrams for both ADH and AHH hydrates in the low-pressure regions might also be contributed to by the semilocal exchange-correlation functional that has been argued to overstabilise ionic structures.[43] This could lead to spurious stabilisation of ADH-I* over ADH-II, and of AMH-$P4/nmm$ over both ADH and AHH. However, the relative stabilities of the different hydrates are qualitatively unaffected for various other exchange-correlation functionals; in the SM we show phase diagrams equivalent to Figure 5 obtained from the LDA functional as well as from dispersion-corrections of the Grimme (D2), Tkatchenko-Scheffler (TS), and many-body dispersion (MBD) type.[59–61] While the density-based dispersion corrections of the vdW-DF2 type (e.g., in the form of revPBE-vdW2) and the meta-GGA SCAN functional have been shown to give very good results for the high-pressure phase sequence of molecular ices,[62–64], it is not clear whether this also applies to other molecules, and mixtures such as those studied here. For hydrogen hydrates, the PBE functional returns more accurate phase stabilities than dispersion corrections of the vdW-DF type,[65, 66], while for noble gas hydrates it shows less overbinding than any dispersion-corrected functional.[67] At pressures beyond the molecular phases (from 10's to 100's of GPa, as considered here) the semilocal description of PBE should become even more appropriate, as electron densities tend to become more uniform,[68] and non-bonded interactions become very similar amongst competing quasi-close-packed structures.[69]

Ionic motifs under pressure. Across all phases, ionization emerges as a clear pathway towards stability with increased pressure. All newly presented phases in the known hydrate stoichiometries, as well as the new ammonia quarterhydrate, benefit from proton transfer from water to ammonia. If the overall composition permits, water molecules tend to be fully deprotonated and the hydrates then comprise ionic motifs of the form $O^{2-}\cdot(NH_4^+)_2$ or

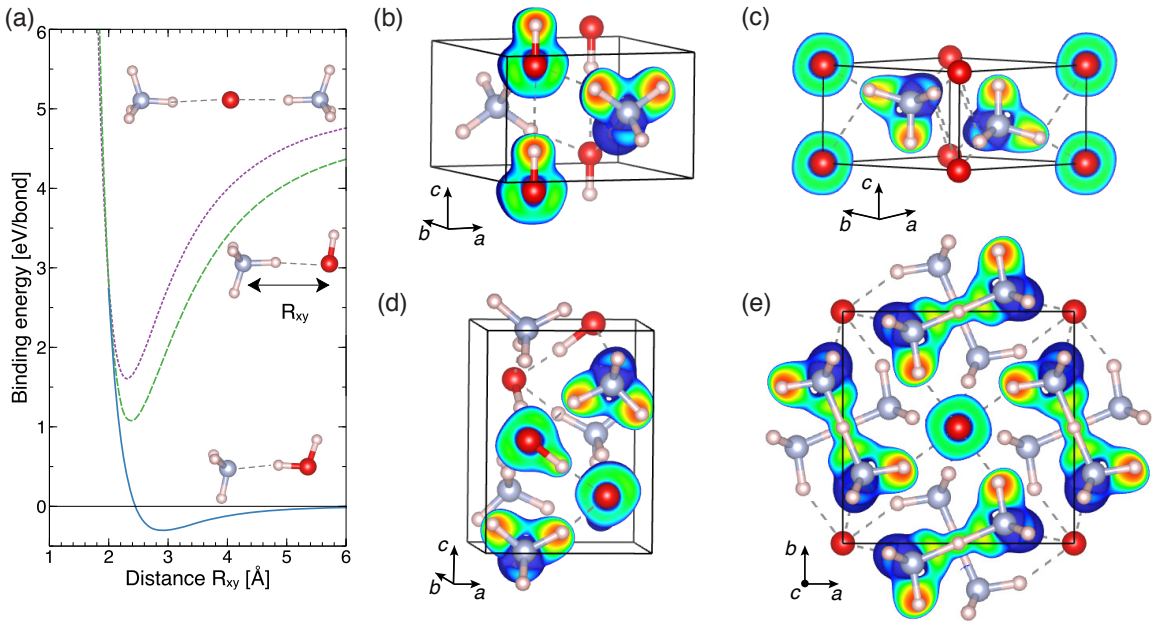

FIG. 6. (a) Binding energies of water-ammonia dimers and trimers from PBE calculations (geometries shown as insets), relative to neutral gas phase molecules, and normalized per hydrogen bond. Blue solid line: $HOH\cdots NH_3$; green dashed line: $H_3NH\cdots OH$; purple dotted line: $H_3NH\cdots O\cdots HNH_3$. (b-e) Isosurfaces of the electron localisation function (ELF=0.7) in ammonia hydrates, together with cross sections from ELF=0.7 (blue) to ELF=1.0 (red): (b) AMH-$P4/nmm$ at 10 GPa, (c) AHH-$P\bar{3}m1$ at 200 GPa, (d) AMH-$P4_3$ at 100 GPa, (e) AQH-$I4/m$ at 100 GPa. All structures drawn to the same scale. Hydrogen bonds are indicated by dashed lines.

$O^{2-}\cdot(N_2H_7^+)_2$ that are supported by copious hydrogen bonding. The hydronitrogen cations are very stable; none are predicted to undergo changes until the hydrates themselves decompose. To quantify the energetics of successive deprotonation of water molecules we performed molecular calculations on selected water-ammonia dimers and trimers. In the gas phase (at large separations), the proton transfer reaction $H_2O + NH_3 \rightarrow OH^- + NH_4^+$ is endothermic by about 8 eV. The second proton transfer, resulting in $O^{2-} + 2NH_4^+$, costs another 16 eV. However, electrostatic attraction largely makes up for this cost, as shown in Figure 6(a). The minima of the potential energies of the ionic hydrogen-bonded $H_3NH\cdots OH$ dimer and the $H_3NH\cdots O\cdots HNH_3$ trimer are only 1.4 and 1.9 eV per hydrogen bond above the minimum of the neutral $HOH\cdots NH_3$ dimer. These metastable minima occur at smaller R_{N-O} separations than the most stable minimum but, crucially, these ionised structures have lower

energies than the neutral dimer at the smallest separations: along the repulsive part of the potential energy surface, fully de-protonated water is the most stable configuration. While these molecular models can not by themselves explain the behaviour of extended phases – where mutual coordination, global packing, and other energy contributions are significant – they corroborate the trends seen throughout this work.

The chemical interpretations are further supported by topological real-space analyses of the electronic charge density and the electron localization function (ELF).[28, 70, 71] In Figure 6(b-e) we show ELF isosurfaces and cross sections for some of the most relevant structures across the different hydrates. These support the interpretation of the various atomic and ionic molecular units: AMH structures feature localised NH_4^+ and OH^- groups, the latter with the typical ring structure of the lone pairs around oxygen; AHH and AQH feature near-spherical isolated oxygen anions and counterions NH_4^+ and $N_2H_7^+$, respectively.

A quantitative topological analysis of the same data is tabulated in the SM. The covalent N–H and O–H bonds (where present) hold roughly 2.0 and 1.6 electrons each; the respective interpretations as bound NH_4 and OH units are justified. The partial charges on NH_4 ($+0.65\cdots0.74$ electrons), N_2H_7 (+0.655), OH ($-0.68\cdots-0.74$ electrons) and O (-1.3 electrons) are consistent with formal charges of +1, -1, and -2, respectively (in NaCl the same analysis yields ±0.85 electrons per ion). The dashed lines shown e.g. in Figure 6(b-e) all have bond interaction points (b.i.p.'s) along the respective (O/N)-H$\cdots$(O/N) connections but these have low ELF values between 0.05 and 0.5; this is consistent with their interpretation as hydrogen bonds, the strength of which correlates to those ELF values. An extreme case appears on the N_2H_7 subunit, where the central proton has its own detached monosynaptic basin with a population of 0.42 e^- and is strongly connected to the N atoms either side (ELF=0.848 at the b.i.p.). Therefore, this symmetrical very strong hydrogen bond can be considered as a true chemical bond. A similar bonding image has been found in ice X along the O-H-O line.[72] A Bader analysis, based purely on the topology of the electron density, gives analogous results (see the SM): partial charges on the different subunits are consistent with their formal charges stated throughout; strong covalent bonds exist within the subunits (with high densities, strongly negative Laplacians at the bond points), and they are connected by multiple hydrogen bonds (with low densities, weakly positive Laplacians at the bond points).

IV. CONCLUSIONS

We present a comprehensive computational study across the entire binary composition range of ammonia-water mixtures, as function of compression. We have found a series of new phases stable in ammonia monohydrate, AMH, and dihydrate, ADH, that change the picture of the high-pressure stability of both compounds. By sampling arbitrary binary ammonia-water mixtures we predict a new ammonia-rich hydrate, ammonia quarterhydrate or AQH, to become stable in an experimentally accessible pressure range. AQH features the unusual $N_2H_7^+$ cation above 60 GPa.

Compounds where proton transfer from water to ammonia is limited by the number of acceptor ammonia molecules (ADH and AMH) are stable only up to moderate pressures, below 1 Mbar, whereas compounds that allow full deprotonation of water (AHH and AQH) are stable to much higher pressures. The latter compounds feature cationic hydronitrogens, NH_4^+ and $N_2H_7^+$, that persist until the respective hydrates are predicted to decompose completely. Mixtures of ammonia and water thus choose a unique chemical response to compression: they combine water's propensity to give up its protons with ammonia's tendency to form ionized hydrogen-bonded structures, in a way not seen in either of the constituents.

We have shown that it is insufficient to study the phase transformations of individual hydrates, as their respective stability constraints mostly involve other hydrates, and not only the constituent ices. By considering all these decomposition reactions, and finite temperature effects at the harmonic level, we were able to construct the full phase diagram of all ammonia hydrates at specific pressure and temperature conditions. This phase diagram shows reasonable agreement with experiment regarding stabilities, phase transitions, and decomposition reactions amongst molecular hydrate phases at low pressures, even though the roles of DMA phases and unresolved hydrate structures such as AMH-IV and ADH-IV should be explored further.

At high pressures, the formation of fully ionic solids will have consequences for the finite temperature behavior of these phases. If strongly bound molecular cation motifs persist up to high pressures, partial melting of the mixtures (e.g. the formation of superionic phases) might be shifted to higher temperatures, or even replaced by formation of ionic molecular liquids upon melting. This in turn will influence thermal and electric conductivities of any such mixture along icy planet isentropes.

The trend that emerges here with pressure, towards the formation of ammonia-*rich* hydrates, is intriguing, as it runs counter to the cosmic abundance ratio of ammonia and water. It could suggest that all ammonia-water mixtures separate into water ice and ammonia-rich hydrates under sufficient compression. The latter would always be less gravimetrically dense than pure water ice and could therefore contribute to more complex inner structures in the mantles of icy planets than hitherto considered.

V. SUPPLEMENTARY MATERIAL

Additional data on crystallographic information for all compounds, zero-point energies, Gibbs free energies, phonon dispersions, topological ELF and charge analyses, simulated IR/Raman frequencies, and phase diagrams from different exchange-correlation functionals can be found in the Supplemental Material to this paper. Data reported in this paper has also been deposited, in compliance with EPSRC open research data policy, on The University of Edinburgh repository https://datashare.is.ed.ac.uk.

ACKNOWLEDGMENTS

This research was supported by the UK's EPSRC through the Condensed Matter Centre for Doctoral Training (EP/L015110/1). Computational resources provided by the UK's National Supercomputer Service through the UK Car-Parrinello consortium (EP/P022561/1) and project ID d56 "Planetary Interiors", by the UK Materials and Molecular Modelling Hub (EP/P020194) and by the Royal Society (RG-150247) are gratefully acknowledged. M. Marqués acknowledges support from ERC grant HECATE. Y. Wang and Y. Ma acknowledge the funding support from National Natural Science Foundation of China under Grant No. 11534003 and National Key Research and Development Program of China under Grant No. 2016YFB0201200.

[1] W. B. Hubbard and J. J. MacFarlane, J. Geophys. Res. Solid Earth **85**, 225 (1980).

[2] M. Ross, Nature **292**, 435 (1981).

[3] L. A. Young, S. A. Stern, H. A. Weaver, F. Bagenal, R. P. Binzel, B. Buratti, A. F. Cheng, D. Cruikshank, G. R. Gladstone, W. M. Grundy, D. P. Hinson, M. Horanyi, D. E. Jennings, I. R. Linscott, D. J. McComas, W. B. McKinnon, R. McNutt, J. M. Moore, S. Murchie, C. B. Olkin, C. C. Porco, H. Reitsema, D. C. Reuter, J. R. Spencer, D. C. Slater, D. Strobel, M. E. Summers, and G. L. Tyler, Space Sci. Rev. **140**, 93 (2008).

[4] Y. Sekine, H. Genda, S. Sugita, T. Kadono, and T. Matsui, Nat. Geosci. **4**, 359 (2011).

[5] L. Noack, I. Snellen, and H. Rauer, Space Sci. Rev. , 877 (2017).

[6] L. Zhu, H. Liu, C. J. Pickard, G. Zou, and Y. Ma, Nat. Chem. **6**, 644 (2014).

[7] A. Hermann and P. Schwerdtfeger, J. Phys. Chem. Lett. **5**, 4336 (2014).

[8] A. Hermann, in *Rev. Comput. Chem.*, edited by A. L. Parrill and K. B. Lipkowitz (John Wiley & Sons Inc., Hoboken, NJ, 2017) pp. 1–41.

[9] J. Liu, Q. Hu, D. Young Kim, Z. Wu, W. Wang, Y. Xiao, P. Chow, Y. Meng, V. B. Prakapenka, H.-K. Mao, and W. L. Mao, Nature **551**, 494 (2017).

[10] S. C. Zhu, Q. Hu, W. L. Mao, H. K. Mao, and H. Sheng, J. Am. Chem. Soc. **139**, 12129 (2017).

[11] L. R. Benedetti, J. H. Nguyen, W. A. Caldwell, H. Liu, M. Kruger, and R. Jeanloz, Science **286**, 100 (1999).

[12] C. Cavazzoni, G. L. Chiarotti, S. Scandolo, E. Tosatti, M. Bernasconi, and M. Parrinello, Science **283**, 44 (1999).

[13] Y. Wang, H. Liu, J. Lv, L. Zhu, H. Wang, and Y. Ma, Nat. Commun. **2**, 563 (2011).

[14] A. Hermann, N. W. Ashcroft, and R. Hoffmann, Proc. Natl. Acad. Sci. U. S. A. **109**, 745 (2012).

[15] T. Palasyuk, I. Troyan, M. Eremets, V. Drozd, S. Medvedev, P. Zaleski-Ejgierd, E. Magos-Palasyuk, H. Wang, S. A. Bonev, D. Dudenko, and P. Naumov, Nat. Commun. **5**, 3460 (2014).

[16] S. Ninet, F. Datchi, P. Dumas, M. Mezouar, G. Garbarino, A. Mafety, C. J. Pickard, R. J. Needs, and A. M. Saitta, Phys. Rev. B **89**, 174103 (2014).

[17] A. F. Goncharov, V. V. Struzhkin, M. S. Somayazulu, R. J. Hemley, and H. K. Mao, Science **273**, 218 (1996).

[18] M. Benoit, M. Bernasconi, P. Focher, and M. Parrinello, Phys. Rev. Lett. **76**, 2934 (1996).

[19] C. J. Pickard and R. J. Needs, Nat. Mater. **7**, 775 (2008).

[20] C. G. Pruteanu, G. J. Ackland, W. C. K. Poon, and J. S. Loveday, Sci. Adv. **3**, e1700240 (2017).

[21] Y. Wang, J. Lv, L. Zhu, and Y. Ma, Phys. Rev. B **82**, 094116 (2010).

[22] Y. Wang, J. Lv, L. Zhu, and Y. Ma, Computer Physics Communications **183**, 2063 (2012).

[23] G.-R. Qian, C.-H. Hu, A. R. Oganov, Q. Zeng, and H.-Y. Zhou, Sci. Rep. **6**, 25947 (2016), arXiv:arXiv:1411.4513v1.

[24] M. Segall, P. J. Lindan, M. a. Probert, C. Pickard, P. Hasnip, S. Clark, and M. Payne, Journal of Physics: Condensed Matter **14**, 2717 (2002).

[25] B. Hammer, L. B. Hansen, and J. K. Nørskov, Physical Review B **59**, 7413 (1999).

[26] G. Kresse and J. Furthmüller, Phys. Rev. B **54**, 11169 (1996).

[27] G. Kresse and D. Joubert, Phys. Rev. B **59**, 1758 (1999).

[28] A. Otero-de-la Roza, E. R. Johnson, and V. Luaña, Comput. Phys. Commun. **185**, 1007 (2014).

[29] M. J. Frisch, G. W. Trucks, H. B. Schlegel, G. E. Scuseria, M. A. Robb, J. R. Cheeseman, G. Scalmani, V. Barone, B. Mennucci, G. A. Petersson, H. Nakatsuji, M. Caricato, X. Li, H. P. Hratchian, A. F. Izmaylov, J. Bloino, G. Zheng, J. L. Sonnenberg, M. Hada, M. Ehara, K. Toyota, R. Fukuda, J. Hasegawa, M. Ishida, T. Nakajima, Y. Honda, O. Kitao, H. Nakai, T. Vreven, J. A. Montgomery Jr., J. E. Peralta, F. Ogliaro, M. Bearpark, J. J. Heyd, E. Brothers, K. N. Kudin, V. N. Staroverov, R. Kobayashi, J. Normand, K. Raghavachari, A. Rendell, J. C. Burant, S. S. Iyengar, J. Tomasi, M. Cossi, N. Rega, J. M. Millam, M. Klene, J. E. Knox, J. B. Cross, V. Bakken, C. Adamo, J. Jaramillo, R. Gomperts, R. E. Stratmann, O. Yazyev, A. J. Austin, R. Cammi, C. Pomelli, J. W. Ochterski, R. L. Martin, K. Morokuma, V. G. Zakrzewski, G. A. Voth, P. Salvador, J. J. Dannenberg, S. Dapprich, A. D. Daniels, Ö. Farkas, J. B. Foresman, J. V. Ortiz, J. Cioslowski, and D. J. Fox, "Gaussian 09 Revision A.02,".

[30] T. H. Dunning, Jr., J. Chem. Phys. **90**, 1007 (1989).

[31] J. S. Loveday and R. J. Nelmes, High Press. Res. **24**, 45 (2004).

[32] A. D. Fortes and M. Choukroun, Space Sci. Rev. **153**, 185 (2010).

[33] M. Asplund, N. Grevesse, A. J. Sauval, and P. Scott, Annu. Rev. Astron. Astrophys. **47**, 481 (2009), arXiv:0909.0948.

[34] A. D. Fortes, I. G. Wood, M. Alfredsson, L. Vočadlo, K. S. Knight, W. Marshall, M. Tucker, and F. Fernandez-Alonso, High Press. Res. **27**, 201 (2007).

[35] A. D. Fortes, I. G. Wood, L. Vočadlo, K. S. Knight, W. G. Marshall, M. G. Tucker, and F. Fernandez-Alonso, J. Appl. Crystallogr. **42**, 846 (2009).

[36] C. W. Wilson, C. L. Bull, G. Stinton, and J. S. Loveday, J. Chem. Phys. **136**, 094506 (2012).

[37] J. S. Loveday and R. J. Nelmes, Phys. Rev. Lett. **83**, 4329 (1999).

[38] J. S. Loveday, R. J. Nelmes, C. L. Bull, H. E. Maynard-Casely, and M. Guthrie, High Press. Res. **29**, 396 (2009).

[39] C. W. Wilson, C. L. Bull, G. W. Stinton, D. M. Amos, M.-E. Donnelly, and J. S. Loveday, J. Chem. Phys. **142**, 094707 (2015).

[40] C. Liu, A. Mafety, J. A. Queyroux, C. W. Wilson, H. Zhang, K. Béneut, G. Le Marchand, B. Baptiste, P. Dumas, G. Garbarino, F. Finocchi, J. S. Loveday, F. Pietrucci, A. M. Saitta, F. Datchi, and S. Ninet, Nat. Commun. **8**, 1065 (2017).

[41] A. D. Fortes, J. P. Brodholt, I. G. Wood, L. Vocadlo, and H. D. B. Jenkins, J. Chem. Phys. **115**, 7006 (2001).

[42] A. D. Fortes, *Computational and experimental studies of solids in the ammonia-water system*, Ph.D. thesis, University College London (2004).

[43] G. I. Griffiths, A. J. Misquitta, A. D. Fortes, C. J. Pickard, and R. J. Needs, J. Chem. Phys. **137**, 064506 (2012), arXiv:arXiv:1112.2636v1.

[44] X. Jiang, X. Wu, Z. Zheng, Y. Huang, J. Zhao, and S. Information, Phys. Rev. B **95**, 144104 (2017).

[45] C. Ma, F. Li, Q. Zhou, F. Huang, J. Wang, M. Zhang, Z. Wang, and Q. Cui, RSC Advances **2**, 4920 (2012).

[46] J. S. Loveday and R. J. Nelmes, in *Sci. Technol. High Press. Proc. AIRAPT-17*, edited by M. H. Manghnani, W. J. Nellis, and M. F. Nicol (Universities Press, Hyderabad, India, 2000) pp. 133–136.

[47] A. D. Fortes, E. Suard, M. H. Lemée-Cailleau, C. J. Pickard, and R. J. Needs, J. Am. Chem. Soc. **131**, 13508 (2009).

[48] M. Bethkenhagen, D. Cebulla, R. Redmer, and S. Hamel, J. Phys. Chem. A , 10582 (2015).

[49] A. Hermann, N. W. Ashcroft, and R. Hoffmann, J. Chem. Phys. **141**, 024505 (2014).

[50] A. Hermann, Phys. Chem. Chem. Phys. **18**, 16527 (2016).

[51] G. I. G. Griffiths, A. D. Fortes, C. J. Pickard, and R. J. Needs, J. Chem. Phys. **136**, 174512 (2012).

[52] V. Naden Robinson, Y. Wang, Y. Ma, and A. Hermann, Proc. Natl. Acad. Sci. **114**, 9003 (2017).

[53] M. L. Troost, Compt. rend. **92**, 715 (1881).

[54] G. W. Watt and W. R. McBride, J. Am. Chem. Soc. **77**, 1317 (1955).

[55] H. J. Berthold, W. Preibsch, and E. Vonholdt, Angew. Chem. Int. Ed. Engl. **27**, 1524 (1988).

[56] S. Boone and M. F. Nicol, in *Proc. Lunar Planet. Sci. Conf.* (1991) pp. 603–610.

[57] K. Hermansson, G. Gajewski, and P. D. Mitev, J. Phys. Chem. A **112**, 13487 (2008).

[58] B. Monserrat, N. D. Drummond, and R. J. Needs, Phys. Rev. B **87**, 144302 (2013), arXiv:1303.0745.

[59] S. Grimme, J. Comput. Chem. **27**, 1787 (2006).

[60] A. Tkatchenko and M. Scheffler, Phys. Rev. Lett. **102**, 073005 (2009).

[61] A. Ambrosetti, A. M. Reilly, R. A. DiStasio, and A. Tkatchenko, J. Chem. Phys. **140**, 18A508 (2014).

[62] B. Santra, J. Klimeš, A. Tkatchenko, D. Alfè, B. Slater, A. Michaelides, R. Car, and M. Scheffler, J. Chem. Phys. **139**, 154702 (2013).

[63] M. J. Gillan, D. Alfe, and A. Michaelides, J. Chem. Phys. **144**, 130901 (2016), arXiv:1603.01990 [cond-mat.mtrl-sci].

[64] J. Sun, R. C. Remsing, Y. Zhang, Z. Sun, A. Ruzsinszky, H. Peng, Z. Yang, A. Paul, U. Waghmare, X. Wu, M. L. Klein, and J. P. Perdew, Nat. Chem. **8**, 831 (2016).

[65] P. Teeratchanan, *First-principles studies of gas hydrates and clathrates under pressure*, Ph.D. thesis, The University of Edinburgh (2017).

[66] J. Košata, P. Merkl, P. Teeratchanan, and A. Hermann, J. Phys. Chem. Lett. **9**, 5624 (2018).

[67] P. Teeratchanan and A. Hermann, J. Chem. Phys. **143**, 154507 (2015).

[68] M. Martinez-Canales, C. J. Pickard, and R. J. Needs, Phys. Rev. Lett. **108**, 045704 (2012).

[69] A. Hermann, N. W. Ashcroft, and R. Hoffmann, Phys. Rev. B **88**, 214113 (2013).

[70] A. D. Becke and K. E. Edgecombe, J. Chem. Phys. **92**, 5397 (1990).

[71] A. Savin, O. Jepsen, J. Flad, O. K. Andersen, H. Preuss, and H. G. von Schnering, Angew. Chemie Int. Ed. **31**, 187 (1992).

[72] M. Marqués, G. J. Ackland, and J. S. Loveday, High Press. Res. **29**, 208 (2009).